

Optical observation of the C , $3s\sigma_g F_3$, and $3p\pi_u G_3$ ${}^3\Pi_u$ states of N_2

B. R. Lewis,^{1,a)} K. G. H. Baldwin,¹ J. P. Sprengers,² W. Ubachs,² G. Stark,³ and K. Yoshino⁴

¹Research School of Physical Sciences and Engineering, The Australian National University, Canberra, Australian Capital Territory 0200, Australia

²Department of Physics and Astronomy, Laser Centre, Vrije Universiteit, De Boelelaan 1081, 1081 HV Amsterdam, The Netherlands

³Department of Physics, Wellesley College, Wellesley, Massachusetts 02481, USA

⁴Harvard-Smithsonian Center for Astrophysics, Cambridge, Massachusetts 02138, USA

(Received 23 June 2008; accepted 4 September 2008; published online 24 October 2008)

High-resolution laser-based one extreme-ultraviolet (EUV)+one UV two-photon ionization spectroscopy and EUV photoabsorption spectroscopy have been employed to study spin-forbidden ${}^3\Pi_u$ - X ${}^1\Sigma_g^+(v,0)$ transitions in ${}^{14}N_2$ and ${}^{15}N_2$. Levels of the C ${}^3\Pi_u$ valence and $3s\sigma_g F_3$ and $3p\pi_u G_3$ ${}^3\Pi_u$ Rydberg states are characterized, either through their direct optical observation, or, indirectly, through their perturbative effects on the ${}^1\Pi_u$ and ${}^1\Sigma_u^+$ states, which are accessible in dipole-allowed transitions. Optical observation of the G_3 - $X(0,0)$ and $(1,0)$ transitions is reported for the first time, together with evidence for six new vibrational levels of the C state. Following the recent observation of the F_3 - $X(0,0)$ transition at rotational resolution [J. P. Sprengers et al., *J. Chem. Phys.* **123**, 144315 (2005)], the $F_3(v=1)$ level is found to be responsible for a local perturbation in the rotational predissociation pattern of the b' ${}^1\Sigma_u^+(v=4)$ state. Despite their somewhat fragmentary nature, these new observations provide a valuable database on the ${}^3\Pi_u$ states of N_2 and their interactions which will help elucidate the predissociation mechanisms for the nitrogen molecule.

© 2008 American Institute of Physics. [DOI: [10.1063/1.2990655](https://doi.org/10.1063/1.2990655)]

I. INTRODUCTION

Predissociation of the ${}^1\Pi_u$ electronic states of N_2 , which are accessible in electric-dipole-allowed transitions from the X ${}^1\Sigma_g^+$ ground state, is an important process underlying the photochemistry of nitrogen-rich planetary atmospheres. It has long been known¹⁻³ that the spectroscopy of these excited states is governed by strong Rydberg-valence and Rydberg-Rydberg interactions which cause major energy perturbations and strong intensity interference effects, a pioneering treatment of these interactions having been performed by Stahel *et al.*⁴ However, much less is known of the isoconfigurational ${}^3\Pi_u$ states, which are likely to be affected by similar interactions, but are accessible only in optically forbidden transitions from the ground state. While the importance of the ${}^3\Pi_u$ states to the N_2 predissociation process had also been realized,^{2,5} only recently has a quantitative predissociation model for the lowest-energy ${}^1\Pi_u$ levels, including spin-orbit coupling between the ${}^1\Pi_u$ and ${}^3\Pi_u$ manifolds, been developed.^{6,7} Any further extension of such a predissociation model to higher energies will require a significantly greater understanding of the ${}^3\Pi_u$ states and their interactions than existing presently.

The lowest ${}^3\Pi_u$ valence states of N_2 are the strongly bound C ${}^3\Pi_u$ state, which is isoconfigurational with the b ${}^1\Pi_u$ state, and the weakly bound C' ${}^3\Pi_u$ state. Below $\sim 99\,000$ cm^{-1} , vibrational levels of the C ${}^3\Pi_u$ and C' ${}^3\Pi_u$ states have been well characterized experimentally using conventional spectroscopic techniques, in particular, through

the work of Tilford *et al.*⁸ [$C(v=0-4)$], Ledbetter⁹ [$C(v=5)$], Carroll¹⁰ [$C'(v=0)$], Ledbetter and Dressler¹¹ [$C'(v=1)$], and Tanaka and Jursa¹² [$C'(v=2)$]. Great insight into the structure of these states and their strong mutual electrostatic interaction, which is responsible for rapidly increasing perturbations in the C -state levels as v increases, was first provided in a key paper by Carroll and Mulliken.¹³ The observations of Hori and Endo,¹⁴ who, in high-pressure emission spectra of the C ${}^3\Pi_u$ - B ${}^3\Pi_g$ (second positive) system of N_2 , noticed a complete breaking off in the rotational structure at high J in the $C(v=2-3)$ emissions, were also explained by Carroll and Mulliken¹³ in terms of the electrostatic predissociation of the C state by the C' state, which correlates with the $N(^4S)+N(^2D)$ dissociation limit at $97\,938 \pm 40$ cm^{-1} .¹⁵ Ledbetter and Dressler¹¹ obtained a semiempirical estimate of ~ 700 cm^{-1} for the electrostatic coupling between the C and C' states by means of a two-state deperturbation of experimental term values, while Lewis *et al.*⁶ determined a value of 810 ± 20 cm^{-1} using a coupled-channel analysis of a more extensive data set, including predissociation linewidths for the ${}^1\Pi_u$ levels.

The lowest ${}^3\Pi_u$ Rydberg state of N_2 is the $3p\pi_u$ ${}^3\Pi_u$ state, which is the first member of the $np\pi_u$ Rydberg series converging on the X ${}^2\Sigma_g^+$ state of the molecular ion. The second lowest is the $3s\sigma_g$ ${}^3\Pi_u$ state, which is the first member of the $ns\sigma_g$ Rydberg series converging on the A ${}^2\Pi_u$ first-excited state of the ion. Since before 1971,¹⁶ these states have been known widely as the G and F states, respectively. However, the label G has also been used since 1972 to refer to a valence state,¹⁷ creating some confusion. Here, we pro-

^{a)}Electronic mail: brenton.lewis@anu.edu.au.

pose that the formal labels for the $np\pi_u\ ^3\Pi_u$ and $ns\sigma_g\ ^3\Pi_u$ Rydberg series be G_n and F_n , respectively, consistent with the standard nomenclature for the isoconfigurational singlet states, $np\pi_u c_n\ ^1\Pi_u$ and $ns\sigma_g o_n\ ^1\Pi_u$. Similarly, we propose the labels D_{n+1} for the $np\sigma_u\ ^3\Sigma_u^+$ Rydberg series, consistent with usage for the isoconfigurational singlet states $np\sigma_u c'_{n+1}\ ^1\Sigma_u^+$. Hereafter, for brevity, we will drop the subscripts for the lowest ($n=3$) members of these series, using the G , F , c , o , D , and c' labels, respectively.

Until recently, the only published assignments for vibrational levels of the G and F states had been derived from low-resolution electron-energy-loss^{18–20} and translational kinetic-energy-release (KER)²¹ spectra, with the latter study of van der Kamp *et al.*²¹ the first to assign convincingly the $v=0$ levels of the G and F states. However, in two recent investigations, both the $G(v=0)$ and $F(v=0)$ states have been studied at high resolution, revealing rotational structure for the first time. First, Hashimoto and Kanamori²² performed a near-infrared diode-laser spectroscopic study of the Rydberg-Rydberg transition $G\ ^3\Pi_u-E\ ^3\Sigma_g^+(0,0)$, with a Doppler-limited resolution of $\sim 0.01\ \text{cm}^{-1}$ full width at half maximum (FWHM), enabling rotational analysis and determination of the $>0.1\ \text{cm}^{-1}$ FWHM predissociation linewidth for the $G(v=0)$ state. Second, in measurements related to the work to be presented here, Sprengers *et al.*²³ used two-photon ionization laser spectroscopy, with an effective resolution of $\sim 0.06\ \text{cm}^{-1}$ FWHM, to study the extreme-ultraviolet (EUV) $F\ ^3\Pi_u-X\ ^1\Sigma_g^+(0,0)$ forbidden transition, obtaining spectroscopic parameters and revealing a predissociation linewidth of $\sim 0.45\ \text{cm}^{-1}$ FWHM for the $F(v=0)$ state. When taken together, the results of these two experiments indicate a strong degree of Rydberg-Rydberg electrostatic mixing between the G and F states.²³

Optical observation of the $^3\Pi_u$ states of N_2 is hampered by the spin-forbidden nature of the transitions from the $X\ ^1\Sigma_g^+$ state. In addition, for levels above the $\text{N}(^4S)+\text{N}(^2D)$ dissociation limit, the opportunities to observe $^3\Pi_u$ -state rotational structure are limited by strong predissociation broadening mediated by the C' state. However, due to intensity borrowing from the allowed $^1\Pi_u-X$ transitions, facilitated by $^1\Pi_{u1}\sim^3\Pi_{u1}$ spin-orbit coupling, $^3\Pi_u-X$ transitions may become visible due to fortuitous energy degeneracies, such as in the case of the $F-X(0,0)$ transition.²³ In addition, since the C' state predissociates the C state in an outer-limb crossing, the expected oscillatory structure of the resultant predissociation pattern may lead to some relatively narrow, and hence more readily observable, C -state levels at higher energies. Finally, due to the high density of states, differing rotational constants for the valence and Rydberg states, and prevalent electrostatic, rotational, and spin-orbit interactions, there is an opportunity for the local perturbation of dipole-allowed singlet states by $^3\Pi_u$ states, indirectly providing energetic information on the triplets.

In this work, advantage is taken of the above-mentioned opportunities, with a range of EUV-spectroscopic experimental techniques being employed to provide new information on a number of previously undocumented $^3\Pi_u$ -state levels in $^{14}\text{N}_2$ and $^{15}\text{N}_2$. The levels studied range from rotationally resolved to strongly predissociated, and many of the obser-

vations are fragmentary. Nevertheless, when added to the results of Refs. 22 and 23, a significant new database of experimental spectroscopic and predissociation information results, which should help elucidate the predissociation mechanisms for N_2 over a greater range of energy than possible hitherto. Toward this end, the results of the present work are used in the following companion paper in this issue²⁴ to inform the development of a coupled-channel Schrödinger-equation (CSE) model of the interacting $^3\Pi_u$ Rydberg and valence states of N_2 .²⁵

II. EXPERIMENTAL METHODS

Two distinct experimental techniques were employed. First, high-resolution, EUV laser-based ionization spectroscopy was ideal for the study of longer-lived levels, both for the direct observation of $^3\Pi_u$ levels, and for the study of perturbations in the singlet levels caused by $^3\Pi_u$ states. Second, EUV photoabsorption spectroscopy was suited to the detection of the weakest and/or most strongly predissociated $^3\Pi_u$ levels.

A. EUV laser ionization spectroscopy

The laser-based experiments, performed at the Vrije Universiteit in Amsterdam, employed one EUV+one UV two-photon ionization spectroscopy. Two different EUV sources, based on the sixth harmonic of a pulsed dye laser (PDL) or of a pulsed dye amplifier (PDA), were used. The PDL-based and PDA-based EUV sources have been described in detail elsewhere.^{26,27} Both the PDL and PDA were pumped by the second harmonic of a pulsed neodymium doped yttrium aluminum garnet (Nd:YAG) laser. In addition, the PDA was seeded by the output of a tunable cw ring dye laser, which was in turn pumped by the output of a 532 nm Millennium-V laser. In both systems, the UV radiation was generated by frequency doubling the visible radiation in a KD*P crystal, while the EUV radiation was produced by subsequently frequency tripling the UV radiation in a xenon gas jet. To produce PDA-based EUV radiation in the energy region of 106 000–109 000 cm^{-1} , nonresonant frequency mixing was employed, obeying the relation $\omega_{\text{EUV}}=3\omega_{\text{PDA}}+3\omega_{\text{Nd:YAG}(532)}$. This particular experimental system, which we denote by PDA-FM, has been documented previously in Refs. 28 and 29. Absolute frequency calibration was performed in the visible, using a simultaneously recorded I_2 absorption spectrum.^{26,27,29} The EUV radiation produced was crossed with a pulsed and skimmed N_2 jet and the ions formed in the one EUV+one UV two-photon ionization scheme were accelerated in a time-of-flight setup toward the electron-multiplier detector, enabling separation of the isotopic N_2 spectra.

The absolute wavenumber uncertainty for the EUV lines recorded with the PDL-based system is $\pm 0.2\ \text{cm}^{-1}$, while that for the PDA-based source is $\pm 0.003\ \text{cm}^{-1}$. For those PDA spectra showing significant lifetime and/or Doppler broadening, the uncertainty increases to $\pm 0.02\ \text{cm}^{-1}$. In the case of the PDA-FM source, the EUV wavenumber uncertainty is $\pm 0.01\ \text{cm}^{-1}$ for the narrowest spectral lines, while for lines where Doppler broadening is of importance, the

uncertainty is $\pm 0.02 \text{ cm}^{-1}$. Some of the PDA-based measurements were performed with a nozzle-skimmer distance of 150 mm to reduce Doppler broadening. However, due to the low rotational temperature in the N_2 gas expansion, only levels with $J \leq 5$ could be studied in this case. To observe higher- J levels, the nozzle-skimmer distance was reduced to 0 mm in order to increase the signal sensitivity and the rotational temperature of the gas jet, producing, however, also a significant increase in Doppler broadening.²⁷ The experimental resolution achieved in the EUV was $\sim 0.3 \text{ cm}^{-1}$ FWHM for the PDL-based source and $\sim 0.01 \text{ cm}^{-1}$ or $\sim 0.05 \text{ cm}^{-1}$ FWHM, respectively, for the PDA-based sources with 150 or 0 mm nozzle-skimmer distances. Where possible, using a Voigt-profile-fitting procedure with allowance for the instrumental and Doppler broadening, Lorentzian predissociation linewidth components were determined from the PDA-based spectra for individual rotational lines. This procedure was more problematic for spectra measured with a nozzle-skimmer distance of 0 mm, especially for $J'' > 6$, where signal from the N_2 background gas (Doppler width of $\sim 0.25 \text{ cm}^{-1}$ FWHM) contributed strongly to the line intensity.

B. EUV photoabsorption spectroscopy

The photoabsorption experiments employed both synchrotron-based and conventional single-photon absorption spectroscopy, with photoelectric and photographic detections, respectively.

Room-temperature photoelectric recordings of the diffuse $C-X(7,0)$ band discussed in Sec. III A 1 were taken at the NIST SURF-II synchrotron-radiation facility. A 6.65 m spectrometer equipped with a focal plane scanner provided a resolving power of $\sim 10^5$ when 10 μm entrance and exit slits were used.^{30,31} N_2 , at pressures ranging from 5 to 12 Torr, was admitted to an 11.43 cm absorption cell mounted behind the spectrometer exit slit, with the transmitted EUV radiation detected at $\sim 0.04 \text{ cm}^{-1}$ intervals by a sodium-salicylate-coated photomultiplier. Typical signal rates were $\sim 3000 \text{ s}^{-1}$. Spectra were first corrected for scattered light, typically $\sim 12\%$ of the total signal, and then converted into absolute photoabsorption cross sections through application of the Beer–Lambert law. Wavelength calibration was provided indirectly by the high- J lines of the $b-X(1,0)$ band which, at room temperature, conveniently overlap the scanned region near $101\,000 \text{ cm}^{-1}$. Uncertainties in the N_2 column densities, the scattered light levels, and the background continuum levels result in an estimated uncertainty of $\sim 15\%$ in the experimental integrated cross section.

Photographic recordings of $^{14}N_2$ and $^{15}N_2$ absorption features in the $100\,000$ – $120\,000 \text{ cm}^{-1}$ region were made, at temperatures of 77 and 295 K, on the 6.65 m vacuum spectrograph at Harvard University. With a 10 μm entrance slit, a resolving power of $\sim 2.0 \times 10^5$ was achieved in the second order of a 1200 grooves mm^{-1} grating. The EUV background continuum was provided by a helium discharge source. A 20 cm, windowless absorption cell, which could be cooled by liquid nitrogen (LN_2), was mounted between the discharge and the spectrograph entrance slit. Weaker features

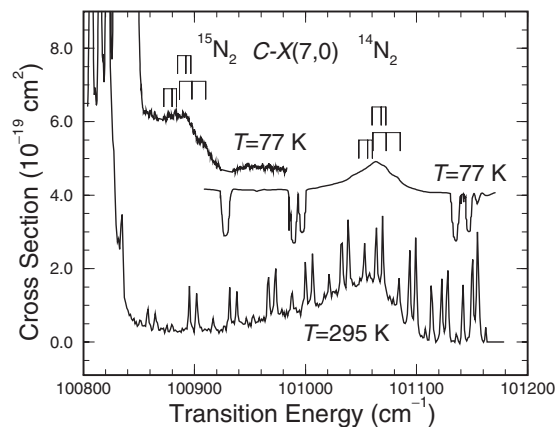


FIG. 1. EUV photoabsorption spectra for the diffuse $C^3\Pi_u-X^1\Sigma_g^+(7,0)$ band of N_2 . Lowest curve: Room-temperature absolute cross section for $^{14}N_2$ from synchrotron-based measurement. The overlapping narrow features are high- J lines from the $b^1\Pi_u-X^1\Sigma_g^+(1,0)$ band. Middle curve: LN_2 -temperature spectrum for $^{14}N_2$, in arbitrary units and displaced upwards for clarity, obtained from a spectrographic plate. The negative features are OI emission lines. Upper curve: LN_2 -temperature spectrum for $^{15}N_2$, in arbitrary units, obtained from a spectrographic plate. Some discrete features have been removed from the spectrum which has been displaced upwards for clarity. In the case of this isotopomer, the diffuse band appears as a shoulder on the $b^1\Pi_u-X^1\Sigma_g^+(0,0)$ band head. Positions of the R -, Q -, and P -branch heads for each of the three subbands, deduced from the fitted spectroscopic constants (see text), are also indicated.

were recorded, at 295 K only, with the spectrograph tank serving as a long-path absorption cell. Unless stated otherwise, all photographic spectra were wavelength calibrated by CO $A-X$ emission bands, recorded in first order on the Kodak SWR plates.

III. RESULTS AND DISCUSSION

The electronic and vibrational assignments of the states that are the subject of this work cannot be established rigorously using only the experimental spectra. The spectroscopic assignments given below are supported by *ab initio* calculations, in the case of the C state,³² and CSE analyses.^{6,24}

A. The $C^3\Pi_u$ state

1. $C^3\Pi_u(v=7)$ in $^{14}N_2$ and $^{15}N_2$

In the lower part of Fig. 1, the absolute $^{14}N_2$ photoabsorption cross section in the region just above the $b-X(0,0)$ band head, measured at room temperature using the synchrotron-based source, is shown. A red-degraded, diffuse feature can be seen, with a peak near $101\,060 \text{ cm}^{-1}$, underlying the narrow, high- J lines from the $b-X(1,0)$ band. By removing the discrete lines from the experimental spectrum and integrating the cross section over the range of $101\,117$ – $101\,887 \text{ cm}^{-1}$, an oscillator strength $f=1.9(3) \times 10^{-5}$ can be deduced for this diffuse band. Diffuse features are also seen in photographic LN_2 -temperature spectra taken in the same region, shown for the cases of $^{14}N_2$ and $^{15}N_2$, in the middle and upper parts of Fig. 1, respectively. The $^{15}N_2$ feature appears as a shoulder on the $b-X(0,0)$ band head, near $100\,890 \text{ cm}^{-1}$.

The low oscillator strength and red shading of the diffuse band in the room-temperature spectrum of Fig. 1 suggest an

electric-dipole-forbidden transition to a valence state with a significantly smaller rotational constant than that of the ground state, $B''=1.99\text{ cm}^{-1}$. Comprehensive *ab initio* calculations³³ indicate that only four such states are expected to possess bound levels in the scanned region, namely, $a' \ ^1\Sigma_u^-$, $w \ ^1\Delta_u$, $B' \ ^3\Sigma_u^-$, and $C \ ^3\Pi_u$. The first two of these can be eliminated as candidates for the upper state in the observed transition since they possess no first-order coupling mechanisms to the $^1\Sigma_u^+$ and $^1\Pi_u$ states which would allow them to borrow significant oscillator strength from the allowed transitions of N_2 in this region. The $B' \ ^3\Sigma_u^-$ state can also be eliminated since it has no electrostatic interactions with other states of like symmetry in the region, which would be necessary in order to allow strong enough predissociation to explain the observed degree of diffuseness, thus leaving the $C \ ^3\Pi_u$ state as the likely upper state in the observed transition. The $C \ ^3\Pi_u$ state has an allowed spin-orbit coupling with the isoconfigurational $b \ ^1\Pi_u$ state,⁶ providing the required intensity-borrowing mechanism, and is known to interact electrostatically with the repulsive limb of the $C' \ ^3\Pi_u$ state,⁶ providing the necessary strong predissociation mechanism. The diffuse bands of Fig. 1 have been used to help construct a CSE model of the predissociation of the lower $^1\Pi_u$ levels of N_2 in Ref. 6, which showed that these bands represent the $C-X(7,0)$ transition.

It is possible to deduce somewhat crude spectroscopic constants for the $C(v=7)$ level from the LN_2 spectra of Fig. 1 by noting that each spectrum reveals a number of very weak substructures, especially a definite *R*-branch head at higher energy than the peak, which also is evident in the underlying room-temperature spectrum. In the case of $^{14}\text{N}_2$, where the nuclear-spin statistics dictate 2:1 even/odd intensity alternation, if the shoulder at $101\,082.8\text{ cm}^{-1}$ is assigned to the highest-energy *R* head [$R(3-5)$], the weak shoulder at $101\,072.3\text{ cm}^{-1}$ to the central-component *R* head [$R(0-3)$], the main peak at $101\,063.4\text{ cm}^{-1}$ to the central *Q*(2) line, and the weak shoulder at $101\,041.8\text{ cm}^{-1}$ to the lowest-energy *Q*(4) line, then fitting of the corresponding $C(v=7)$ terms to the $^3\Pi$ Hamiltonian of Brown and Merer³⁴ yields the following results: $\nu_0=101\,066(1)\text{ cm}^{-1}$, $B=1.38(2)\text{ cm}^{-1}$, and $A=11(2)\text{ cm}^{-1}$.³⁵ In the case of $^{15}\text{N}_2$, with 3:1 odd/even intensity alternation, if the shoulders at $100\,907.0$ and $100\,910.1\text{ cm}^{-1}$ are assigned to the highest-energy *R*(3) and *R*(5) lines, respectively, a possible weak shoulder at $100\,898.6\text{ cm}^{-1}$ to the central-component *R*(1) line, the main peak components at $100\,891.8$ and $100\,883.0\text{ cm}^{-1}$ to the central *Q*(1) and *Q*(3) lines, respectively, and a possible weak peak at $100\,859.8\text{ cm}^{-1}$ to the lowest-energy *Q*(5) line, then the fitted constants are $\nu_0=100\,890(2)\text{ cm}^{-1}$, $B=1.31(2)\text{ cm}^{-1}$, and $A=11(3)\text{ cm}^{-1}$. The corresponding isotopic shift, $176(3)\text{ cm}^{-1}$, is in reasonable agreement with the CSE value of Ref. 6 (162 cm^{-1}), confirming the vibrational assignment. Finally, by profile fitting the LN_2 spectra of Fig. 1, assuming the above constants and a *J*-independent predissociation linewidth Γ for each isotopomer, estimates of $\Gamma=16(3)\text{ cm}^{-1}$ FWHM for $^{14}\text{N}_2$ and $\Gamma=15(3)\text{ cm}^{-1}$ FWHM for $^{15}\text{N}_2$ are obtained, reducing somewhat the uncertainty ranges given in Ref. 6.

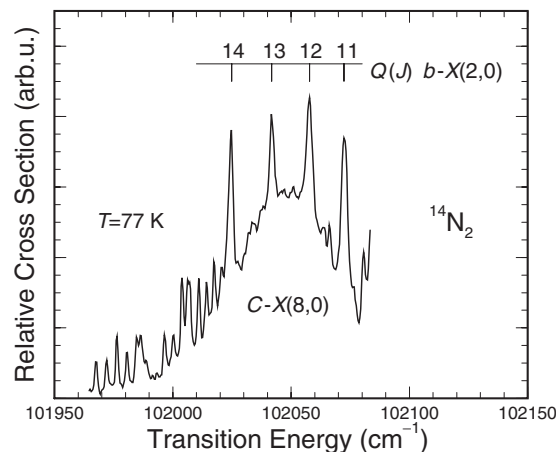


FIG. 2. LN_2 -temperature photoabsorption spectrum for the $C \ ^3\Pi_u-X \ ^1\Sigma_g^+(8,0)$ band of $^{14}\text{N}_2$, obtained from a spectrographic plate. The diffuse band is overlain by discrete rotational lines from the $b-X(2,0)$ band, used for calibration of the energy scale, and the $c'-X(0,1)$ band (Ref. 36).

2. $C \ ^3\Pi_u(v=8)$ in $^{14}\text{N}_2$

The LN_2 -temperature photoabsorption spectrum measured photographically in the region underlying the $b-X(2,0)$ band of $^{14}\text{N}_2$, shown in Fig. 2, indicates a diffuse feature near $102\,050\text{ cm}^{-1}$, which can be associated with the $C-X(8,0)$ transition, following Ref. 6. It is not possible to determine the corresponding oscillator strength because the cross section is neither absolute nor corrected for plate nonlinearity, but visual inspection of a plate containing both bands indicates that the strength of $C-X(8,0)$ exceeds that of $C-X(7,0)$. In addition, the many overlying rotational lines in Fig. 2 prevent a profile analysis of the type performed for the $C-X(7,0)$ bands in Sec. III A 1. However, if it is assumed that the $C-X(8,0)$ and $C-X(7,0)$ bands have a similar structure, then a comparison of the two LN_2 -temperature spectra suggests that $\nu_0=102\,051(3)\text{ cm}^{-1}$ for $C-X(8,0)$ in $^{14}\text{N}_2$ and that the corresponding predissociation linewidth is marginally larger, $\Gamma=18(4)\text{ cm}^{-1}$ FWHM.

3. $C \ ^3\Pi_u(v=13)$ in $^{15}\text{N}_2$

Small irregularities in the rotational structure of the Rydberg $o(v=0)$ level of $^{15}\text{N}_2$ in the range of $J=10-16$ for both *e*- and *f*-parity levels were reported in the laser-based study of Ref. 26, including a noticeable weakening of the *R*(9), *Q*(10), and *P*(11) lines in their PDL-based ionization spectra. PDA-based spectra in the $R(8-11)$ region of the $o-X(0,0)$ band are shown in Fig. 3, confirming the relative weakness of *R*(9) compared with, e.g., *R*(8), especially considering the nuclear-spin statistics in $^{15}\text{N}_2$, which cause the unperturbed odd-*J''* absorption lines to be three times stronger than the even-*J''* lines.

In Fig. 4(a), experimental reduced term values (circles) are shown for the *e*- and *f*-parity levels of $o(v=0)$ in $^{15}\text{N}_2$, obtained from the PDA-based terms of Ref. 26,³⁸ indicating local perturbations by a higher-lying state at $J=10, 12-13$, and $15-16$, with a maximum shift of $\sim 0.15\text{ cm}^{-1}$. The successful detection of such weak perturbations testifies to the spectroscopic precision of the PDA-based laser system. Since the triplet perturber affects both *e*- and *f*-parity levels

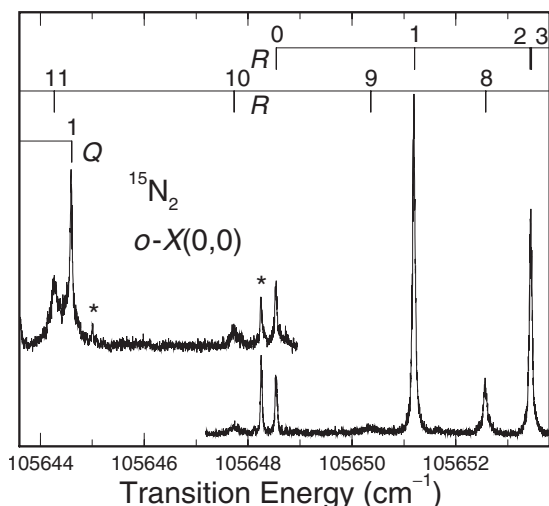


FIG. 3. One EUV+one UV ionization spectra of the $R(8-11)$ region of the $o\ ^1\Pi_u-X\ ^1\Sigma_g^+(0,0)$ band in ${}^{15}\text{N}_2$ recorded with the PDA-based EUV source, demonstrating the weakness of $R(9)$. Lines marked with an asterisk are from the $D\ ^3\Sigma_u^+-X\ ^1\Sigma_g^+(1,0)$ band (Ref. 37). Nozzle-skimmer distance=0 mm.

and has a lower B value than the perturbed Rydberg state, it must be a valence state of ${}^3\Pi_u$ symmetry. The CSE study of Ref. 24 shows that the perturber is $C\ ^3\Pi_u(v=13)$.

In Fig. 4(b), $o(v=0)$ experimental predissociation linewidths (circles) determined from the PDA-based spectra are shown. Despite significant Doppler pedestals in the 0 mm nozzle-skimmer-distance spectra for the corresponding lines (see Sec. II A), we were able to determine that the $J=10e$ and $16e$ levels are broadened significantly. In addition, intensity anomalies in the PDL-based spectrum suggested slight broadening in the $J=12e-13e$ region. The overall predissociation pattern mirrors the maximum level shifts in Fig. 4(a) and is fully consistent with the short-lived $C\ ^3\Pi_u$ perturber approaching Hund's coupling case (b).³⁹

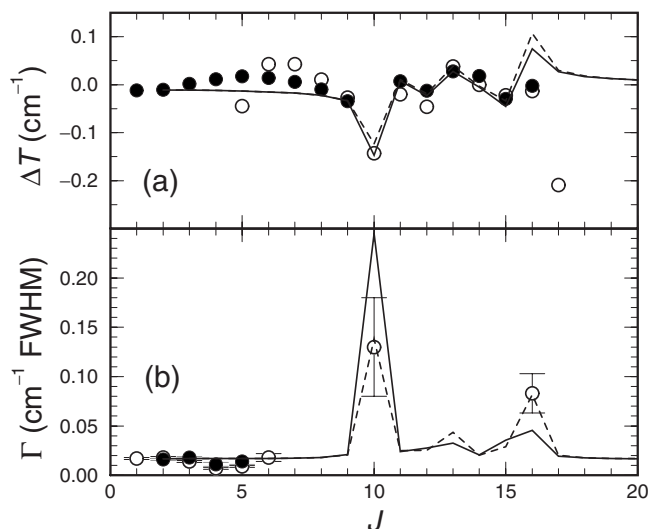


FIG. 4. The local perturbation of $o\ ^1\Pi_u(v=0)$ in ${}^{15}\text{N}_2$ by the higher-lying, shorter-lived $C\ ^3\Pi_u(v=13)$. Predissociation linewidths Γ and reduced term values ΔT from PDA-based spectra (circles) are compared with calculations from a ${}^3\Pi_u\sim{}^1\Pi_u$ interaction model (lines; see text). Open circles and dashed lines refer to the e levels and full circles and solid lines to the f levels. Apart from the main perturbations in the $J=10-16$ region, the e levels at low and high J show signs of additional crossings by $D\ ^3\Sigma_u^+(v=1)$ and $b'\ ^1\Sigma_u^+(v=3)$, respectively.

TABLE I. Spectroscopic parameters, in cm^{-1} , for the deperturbed $C\ ^3\Pi_u(v=13)$ level of ${}^{15}\text{N}_2$ and the $C\ ^3\Pi_u(v=18)$ level of ${}^{14}\text{N}_2$ (see Sec. III A 6), from analysis of their interactions with the $o\ ^1\Pi_u(v=0)$ and $o\ ^1\Pi_u(v=2)$ levels, respectively. 1σ statistical uncertainties resulting from the fitting procedure are given in parentheses, in units of the last significant figure.

Parameter	$C(v=13), {}^{15}\text{N}_2$	$C(v=18), {}^{14}\text{N}_2$
ν_0	105 725(3)	109 725(6)
T_0^a	105 727(3)	109 727(6)
B^b	1.11(2)	1.08(2)
A	-13(3)	-16(4)
Γ^c	2.3(13)	5.0(17)
H_{Co}	0.93(13)	2.7(6)

^aRotationless F_2 energy= ν_0+2B .

^b D was fixed at 0 in the fitting procedure.

^cPredissociation linewidth, in cm^{-1} FWHM.

No extra lines from transitions into the perturbing state are visible in the spectra. Nevertheless, we have managed to simultaneously deperturb the $o(v=0)$ terms and widths using a least-squares fitting procedure based on a complex four-level Hamiltonian that includes unperturbed $o\ ^1\Pi_u(v=0)$ and $C\ ^3\Pi_u(v=13)$ levels, the latter based on a three-parameter version of the ${}^3\Pi$ Hamiltonian of Brown and Merer,³⁴ together with an effective vibronic interaction matrix element $H_{C(13)o(0)}$ between the $\Omega=1$ components. The unperturbed $o(v=0)$ predissociation width, assumed to be J independent, and the unperturbed width for the $C(v=13)$ level, taken to be Ω and J independent, were included as complex terms in the diagonal energy matrix. The results of the fitting procedure are shown in Fig. 4 (lines). As shown in Fig. 4(a), despite the smallness of the shifts, the fitted results are in excellent agreement with the experimental values for $J=6-15$. For $J > 16$, both the e - and f -parity levels of $o(v=0)$ are severely affected by stronger perturbations due to other states, which makes it difficult to define the perturbation at $J=16$ accurately. In the case of the linewidths, the fitted model is also seen in Fig. 4(b) to successfully reproduce the pattern of predissociation, but the finer details cannot be verified without more extensive experimental studies at higher precision. Of primary interest here, the fitted spectroscopic parameters for the $C(v=13)$ level of ${}^{15}\text{N}_2$ are summarized in the second column of Table I. We note that the A value is assumed to be negative (see Sec. III A 4).

4. $C\ ^3\Pi_u(v=14)$ in ${}^{15}\text{N}_2$

In the PDL-based laser-spectroscopic study of Ref. 26, it was noted, without further analysis, that a group of three local perturbations by a higher-lying state occurs in the low- J levels of both e and f parities in the $c\ ^1\Pi_u(v=1)$ Rydberg state of ${}^{15}\text{N}_2$. For the reasons discussed in Sec. III A 3, the perturbing state must be of ${}^3\Pi_u$ symmetry, its identity having been confirmed by the companion study²⁴ as $C\ ^3\Pi_u(v=14)$. Here, we analyze this singlet-triplet perturbation in detail, with the aid of new PDA-based ionization spectra.⁴⁰

In Fig. 5, the PDA-based spectrum in the R -head region of the $c-X(1,0)$ band is shown, demonstrating line-spacing and intensity irregularities, especially in the regions of $R(2-3)$ and $R(6-7)$, together with an extra $R(3)$ line at

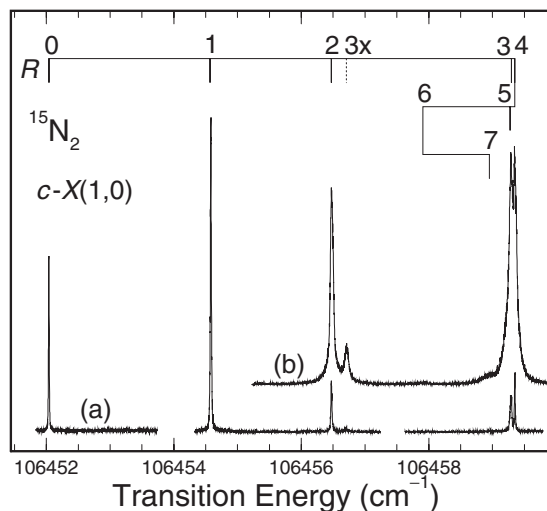


FIG. 5. One EUV+one UV ionization spectrum for the R branch of the $c^1\Pi_u-X^1\Sigma_g^+(1,0)$ band in $^{15}\text{N}_2$, recorded with the PDA-based EUV source. (a) Recordings with nozzle-skimmer distance=150 mm. (b) Recording with nozzle-skimmer distance=0 mm. The rotational structure is irregular due to level crossings with $C^3\Pi_u(v=14)$, the lowest crossing producing a broad extra $R(3)$ line at $106\,456.706\text{ cm}^{-1}$.

$106\,456.706\text{ cm}^{-1}$, arising from the transition into the perturbing $C(v=14, J=4)$ level. An overall examination of the PDA spectra indicates three local perturbations in both the e - and f -parity levels, culminating in the $J=3-4$, $J=7-8$, and $J=10-11$ regions, respectively. Extra lines are observable only in the R and Q branches of the lowest of these perturbations. The $c-X(1,0)$ transition energies determined from the PDA-based spectra are listed in Table II, together with the corresponding $c(v=1)$ terms deduced using $^{15}\text{N}_2$ ground-state terms calculated from the spectroscopic constants of Ref. 41.

Evidence for further rotational structure associated with

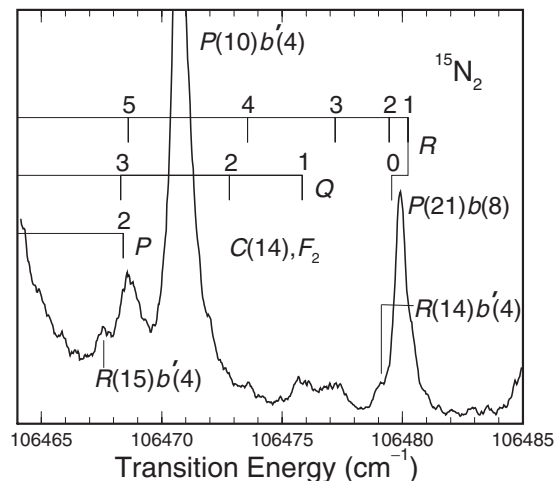


FIG. 6. PDL-based one EUV+one UV ionization spectrum for $^{15}\text{N}_2$ in the region just beyond the R head of the $c^1\Pi_u-X^1\Sigma_g^+(1,0)$ band. Some weak lines, which cannot be assigned as dipole-allowed transitions, have been attributed to the $C^3\Pi_u-X^1\Sigma_g^+(14,0)$ transition. For simplicity, lines are labeled according to the upper state of the relevant transition.

the $C-X(14,0)$ transition can be found in PDL-based spectra in the region just beyond the R head of the $c-X(1,0)$ band. In the example shown in Fig. 6, there are three weak but clear lines not associated with dipole-allowed transitions, which we have assigned as the $Q(1)$, $R(3)$, and (principally) $R(5)$ lines from the central $C-X(14,0)$ subband, which is able to borrow intensity from the nearby $c-X(1,0)$ transition via $c^1\Pi_{u1} \sim C^3\Pi_{u1}$ spin-orbit interaction. The observed $C-X(14,0)$ transition energies and corresponding $C(14)$ terms are summarized in Table III. It is emphasized that some of the lines involved are extremely weak, and the assignments are uncertain, especially for the transitions associated with the highest-energy subband.

Term values for the main and extra f -parity levels in the

TABLE II. PDA-based transition energies for the $c^1\Pi_u-X^1\Sigma_g^+(1,0)$ band of $^{15}\text{N}_2$, together with the corresponding $c^1\Pi_u(v=1)$ term values. Note that $106\,000\text{ cm}^{-1}$ must be added to the tabulated values.

J''	$R(J'')$	$Q(J'')$	$P(J'')$	J'	$T_e(J')$	$T_f(J')$
0	452.040					
1	454.582	448.308		1	452.038	452.023
2	456.473	447.097	440.890	2	458.306	458.243
3	459.297	445.243	436.024	3	467.619	467.534
4	459.352	444.390	430.503	4	481.590	481.541
5	459.278 ^a	440.610	425.868	5	496.503	496.334
6	457.908	436.772	418.497	6	515.005	514.783
7	458.952 ^a	431.826	410.996	7	535.917	535.837
8	456.479	429.360	402.192	8	562.946	563.083
9	453.177	423.209 ^a	395.800	9	590.191	590.355 ^a
10		416.511	385.901	10	620.317	620.790
11	445.968	411.254 ^a	375.190	11	655.805	656.374 ^a
12	439.869	402.685	366.137	12	691.086	692.353
13	432.629	393.808	353.161	13	729.532	731.731
14	424.178	384.035	339.650	14	770.552	773.917
15	414.487	373.227		15	814.060	818.770
16	403.663	361.225		16	860.030	866.131
17	391.881	347.961		17	908.569	915.928
				18	959.848	

^aFrom a shoulder in the spectrum.

TABLE III. Observed transition energies and upper-state term values for the $C\ {}^3\Pi_u-X\ {}^1\Sigma_g^+(14,0)$ band of ${}^{15}\text{N}_2$. Note that $106\,000\text{ cm}^{-1}$ must be added to the tabulated values. Values with two figures after the decimal point are from PDL-based spectra, while those with three figures are from PDA-based spectra.

Ω'	J''	$R(J'')$	$Q(J'')$	$P(J'')$	J'	$T_e(J')$	$T_f(J')$
2	1	462.32 ^a			2	466.04 ^a	
	3	456.706	449.940		3	472.250	472.231
	4		441.796	435.099	4	478.996	478.947
	5		434.179	423.271 ^a	5		489.903
1	1		475.83		1		479.55
	3	477.20			4	499.49	
	4	473.59 ^{a,b}			5	510.74 ^{a,b}	
	5	468.62			6	524.34	
0	3	495.96 ^b			4	518.25 ^b	
	11		406.25 ^a		11		651.37 ^a

^aFrom a shoulder in the spectrum.

^bTentative assignment, from a weak line.

region of the $c(v=1) \sim C(v=14)$ crossing in ${}^{15}\text{N}_2$, taken from Tables II and III, respectively, are shown in a reduced form in Fig. 7 (circles), demonstrating the pattern expected in the case of a singlet Rydberg state perturbed by a triplet valence state. Using a least-squares fitting procedure similar to that described in Sec. III A 3, but without complex terms in this case, we have deperturbed the experimental term values, yielding the $C(v=14)$ spectroscopic parameters listed in Table IV (second column), and the deperturbed terms shown in Fig. 7 (lines). The low B value in Table IV is broadly consistent with expectation for this vibrational level of the C valence state, and the sign of the λ value is as expected for the case of a higher-lying $b\ {}^1\Pi_{u1}$ state pushing down the isoconfigurational $C\ {}^3\Pi_{u1}$ sublevels through an allowed spin-orbit coupling. The fitted effective vibronic coupling $H_{C(14)c(1)} = 3.53\text{ cm}^{-1}$, which leads to the observed local perturbations, is a second-order interaction arising from the $c\ {}^1\Pi_u \sim b\ {}^1\Pi_u$ electrostatic and $b\ {}^1\Pi_{u1} \sim C\ {}^3\Pi_{u1}$ spin-orbit couplings, ~ 800 and 46 cm^{-1} , respectively.⁶

Unfortunately, the dipole-forbidden nature of the $C-X(14,0)$ transition makes it impossible to determine unambiguously whether the $C\ {}^3\Pi_u(v=14)$ state is normal or inverted using the usual method of observing in which sub-

band low- J lines are missing from the rotational structure: The choice of positive or negative A values results in equally good term-value fits. We have chosen the $A < 0$ solution, implying an *inverted* $C\ {}^3\Pi_u(v=14)$ state, despite the fact that the lowest levels of the C state are known to be regular.⁸ The C -state potential-energy curve exhibits an inflection near $R = 1.4\text{ \AA}$ ($v=6-7$),⁶ indicating a strong configurational change, so a change from normal to inverted is feasible for the higher vibrational levels of the C state. This particular choice of $A < 0$ is supported qualitatively by the very small Λ doubling observed in the low-energy triplet component (Table III), and, indirectly, by the relative signs of A and the significant “centrifugal-distortion parameter” A_D in Table IV,⁴² which are consistent with a close perturbation from above by the Rydberg $F\ {}^3\Pi_u(v=1)$ state (see also Sec. III C 2). Confirmation that the $C\ {}^3\Pi_u$ state indeed changes from regular to inverted as v increases is provided by the *ab initio* study in the second companion paper to the present work in the current issue.⁴³

Lorentzian linewidth components, resulting principally from predissociation, were determined from the PDA-based

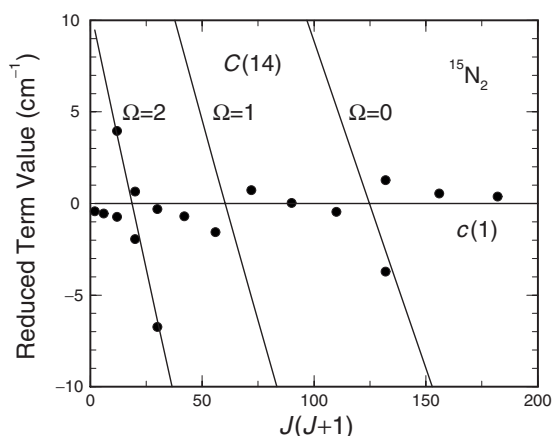


FIG. 7. Reduced term values for f -parity levels in the region of the $c\ {}^1\Pi_u(v=1) \sim C\ {}^3\Pi_u(v=14)$ crossing in ${}^{15}\text{N}_2$. Solid circles: Experimental terms. Solid lines: Deperturbed terms. The term values have been reduced so that the deperturbed $c(v=1)$ levels lie on the zero line.

TABLE IV. Spectroscopic parameters, in cm^{-1} , for the deperturbed $C\ {}^3\Pi_u(v=14)$ level of ${}^{15}\text{N}_2$ and the $C\ {}^3\Pi_u(v=16)$ level of ${}^{14}\text{N}_2$ (see Sec. III A 5). 1σ statistical uncertainties resulting from the fitting procedure are given in parentheses, in units of the last significant figure.

Parameter	$C(v=14), {}^{15}\text{N}_2$	$C(v=16), {}^{14}\text{N}_2$
ν_0 ^a	106 475.9(2)	108 291.8(3)
T_0 ^b	106 477.3(3)	108 293.0(3)
B	1.123(2)	1.153(2)
D	0.000 05(2)	0.0 ^c
A	-14.4(2)	-15.0(1)
A_D	0.031(3)	0.0 ^c
λ	0.72(17)	0.83(8)
λ_D	0.018(5)	0.0 ^c
γ	-0.063(20)	0.0 ^c
o	0.0 ^c	0.69(11)
$H_{C(14)c(1)}$	3.53(4)	
σ_{fit}	0.042	0.12

^aTabulated uncertainties include the calibration uncertainty.

^bRotationless F_2 energy = $\nu_0 - 4\lambda/3 + 2(B - 4\lambda_D/3) - 2\gamma$.

^cParameter fixed during fitting procedure.

TABLE V. Observed Lorentzian linewidths, in cm^{-1} FWHM, for low- J levels of the $c\ ^1\Pi_u(v=1)$ and $C\ ^3\Pi_{u2}(v=14)$ states of $^{15}\text{N}_2$, obtained using the PDA-based system.

State	J	Γ_R	Γ_Q	Γ_P
$c(1)$	1	0.004(2)	0.007(3)	0.005(3)
	2	0.010(3)	0.006(3)	0.009(3)
	3	0.012(4)	0.012(4)	
	4		0.013(4)	
	5	0.005(3)	0.005(3)	
$C(14)$	4	0.049(5)	0.040(6)	

spectra taken with a nozzle-skimmer distance of 150 mm. Results for the low- J levels of $c\ ^1\Pi_u(v=1)$, obtained from independent P -, Q -, and R -branch fits, are summarized in Table V, together with $J=4$ widths for the $C\ ^3\Pi_{u2}(v=14)$ perturber, obtained from fits to the corresponding extra lines. Since only a slight lifetime broadening is observed for the $c(v=1)$ levels, when compared with the instrumental width, the corresponding relative uncertainties in Table V are large.

The $c(v=1)$ linewidth pattern in Table V, which peaks near $J=4$, is broadly consistent with the local perturbation in this region by the $C\ ^3\Pi_{u2}(v=14)$ state, which has a larger linewidth. For $J=4$, at the culmination of the perturbation, the extra-to-main linewidth ratio $\Gamma(C)/\Gamma(c)=3.1(11)$. The mixing coefficients determined in the energy deperturbation procedure discussed above imply that the extra line in this case should have 85% of the strength of the main line. However, the corresponding intensity ratio in the ionization spectrum is observed to be 0.32(5), lower than 0.85 because of the competition between predissociation and ionization, and thus implying a predissociation-width ratio of 2.7(5),⁴⁴ in agreement with the direct width determination but with a lower uncertainty. Unfortunately, because of the significant uncertainties in the $c(v=1)$ linewidths and the measurement of only a single width for $C(v=14)$, it is not possible to perform a meaningful deperturbation of the linewidths. However, it seems safe to assume that $\Gamma(C)=0.03\text{--}0.06\ \text{cm}^{-1}$ FWHM and $\Gamma(c)=0.005\text{--}0.010\ \text{cm}^{-1}$ FWHM, while realizing that the C -state value applies only to the $\Omega=2$ substate, and issues of possibly large J dependencies have been ignored.

A lifetime of 1000(100) ps [$\Gamma=0.0053(5)\ \text{cm}^{-1}$ FWHM] was measured at the R -branch band head for the $c\text{-}X(1,0)$ band of $^{15}\text{N}_2$ in a direct time-domain pump-probe experiment.⁴⁵ The present widths are in agreement, except in the region of the local perturbation where there is greater mixing with the triplet C state. In the pump-probe study,⁴⁵ biexponential decay curves were found for higher- J levels, with components of ~ 1000 and ~ 300 ps. Not only the perturbation described above should be taken into account to help explain the 300 ps component, but also the overlap with the $c'\ ^1\Sigma_u^+(v=1)$ level, which has a lifetime in $^{15}\text{N}_2$ of 310(80) ps.²⁹

5. $C\ ^3\Pi_u(v=16)$ in $^{14}\text{N}_2$

In Fig. 8, the LN_2 -temperature photoabsorption spectrum measured photographically for a portion of the

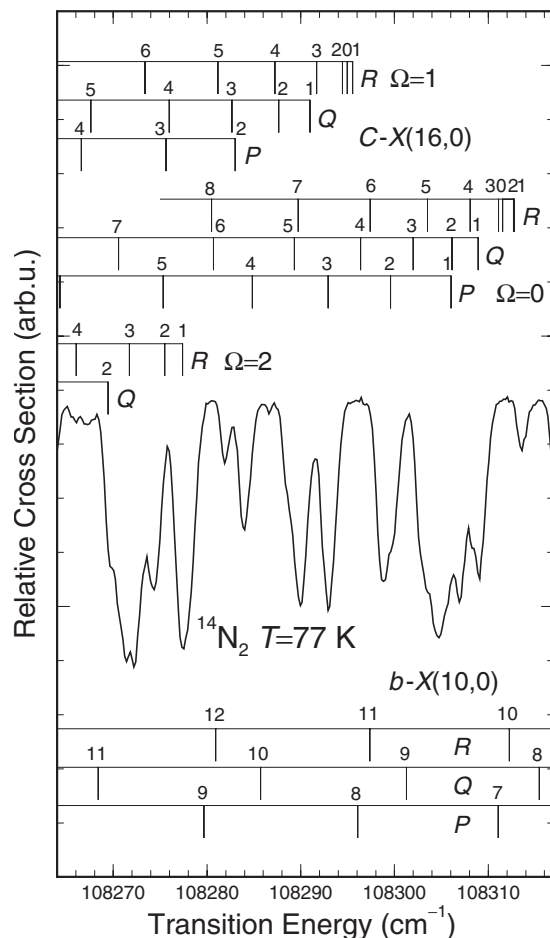


FIG. 8. LN_2 -temperature photoabsorption spectrum in the region of the $b\ ^1\Pi_u\text{-}X\ ^1\Sigma_g^+(10,0)$ band of $^{14}\text{N}_2$, obtained from a spectrographic plate. While the $b\text{-}X(10,0)$ lines are mostly completely saturated, there is additional rotational structure arising from the $C\ ^3\Pi_{u\Omega}\text{-}X\ ^1\Sigma_g^+(16,0)$ subbands, as indicated (see text).

$b\ ^1\Pi_u\text{-}X\ ^1\Sigma_g^+(10,0)$ band of $^{14}\text{N}_2$ is shown, taken at a high enough N_2 pressure to completely saturate most of this band's rotational structure. In the windows of lower absorption between the $b\text{-}X(10,0)$ lines, several additional rotational lines are evident which are neither high- J lines from a higher-lying dipole-allowed transition, nor isotopic lines, since the almost-saturated $b\text{-}X(10,0)$ band head for $^{14}\text{N}^{15}\text{N}$ is near $108\ 265\ \text{cm}^{-1}$, at the extreme left of Fig. 8. The strongest of these additional features can easily be arranged into heavily overlapped, red-degraded R , Q , and P branches associated with a dipole-forbidden transition into a singlet state, but remaining unassigned features near $108\ 307\ \text{cm}^{-1}$ indicate that the upper state of the transition is a multiplet. In the companion paper,²⁴ it is apparent that this newly observed transition corresponds to $C\ ^3\Pi_u\text{-}X\ ^1\Sigma_g^+(16,0)$. Broadly, it can be assumed that the central subband borrows strength from the nearby $b\text{-}X(10,0)$ dipole-allowed transition, through the $C\ ^3\Pi_{u1}(v=16)\sim b\ ^1\Pi_{u1}(v=10)$ spin-orbit interaction, with the much weaker outer subbands gaining strength from the central subband through S -uncoupling rotational interactions within the triplet state. Line assignments and corresponding term values, based on the assumption that $C\ ^3\Pi_u(v=16)$ is inverted, as implied for $C(v=14)$ of $^{15}\text{N}_2$ in Sec. III A 4, are given in Table VI. Spectroscopic param-

TABLE VI. Observed transition energies and upper-state term values for the $C\ {}^3\Pi_u-X\ {}^1\Sigma_g^+(16,0)$ band of ${}^{14}\text{N}_2$. Note that $108\,000\text{ cm}^{-1}$ must be added to the tabulated values.

Ω'	J''	$R(J'')$	$Q(J'')$	$P(J'')$	J'	$T_e(J')$	$T_f(J')$
2	6		234.77		6		318.33
	9	210.68			10	389.71	
1	0	295.07 ^a			1	295.09 ^{b,c}	294.86 ^{a,b}
	1		290.88 ^{a,b}		2	299.68 ^a	299.64 ^b
	2	294.31 ^{a,b}	287.70 ^b	283.17 ^{b,c}	3	306.28 ^d	306.58
	3	291.64 ^a	282.70	275.80 ^a	4	315.55 ^b	315.59 ^a
	4	287.15 ^a	275.80 ^a	266.51 ^d	5	326.94 ^a	327.37 ^{b,d}
	5		267.70 ^{b,d}	255.91 ^b	6		
	6	273.44 ^{b,c}			7	357.00 ^{b,c}	357.05 ^{b,c}
	7		245.64 ^{b,c}		8		375.57 ^b
0	8		232.34 ^b		9		
	10	225.79 ^b			11	444.59 ^b	
	2		306.24		2		318.18
	4	307.97			5	347.76	

^aFrom an unresolved line.

^bFrom a shoulder in the spectrum.

^cFrom a weak line.

^dFrom a weak structure on a heavily absorbed line.

eters, obtained by fitting the Hamiltonian of Ref. 34 to the terms of Table VI, are given in Table IV (third column).

The $C-X(16,0)$ rotational assignments shown in Fig. 8, based on the results of the fitting procedure, are seen to give a good description of the strongest features and even some weak shoulders for the outer subbands which were not deemed strong enough to include in the fit. Overall, the B , A , and λ values for $C(v=16)$ of ${}^{14}\text{N}_2$ in Table IV are quite similar to the deperturbed values for $C(v=14)$ of ${}^{15}\text{N}_2$. However, it was found impossible to explain the two lines near $108\,307\text{ cm}^{-1}$ without including significant Λ doubling in the $\Omega=0$ sublevel, leading to the significant value for o in Table IV. This value is critically dependent on the present choice of assignments in Table VI for the $Q(2)$ and $R(4)$ lines from the $C\ {}^3\Pi_{u0}-X\ {}^1\Sigma_g^+(16,0)$ subband, which is supported by a consideration of their relative intensities.⁴⁶ This Λ doubling can be explained only by spin-orbit coupling between $C\ {}^3\Pi_{u0}$ and a higher ${}^1\Sigma_u^+$ or lower ${}^1\Sigma_u^-$ state. The $b'\ {}^1\Sigma_u^+$ levels are well known and none lie close in energy to $C(v=16)$. Inspection of the potential-energy curves of N_2 implies that a perturbation by a lower-lying vibrational level ($v \approx 35-40$) of the $a'\ {}^1\Sigma_u^-$ state is the likely candidate. This state has a molecular-orbital configuration which differs from the principal C -state configurations by only one electron.³³

6. $C\ {}^3\Pi_u(v=18)$ in ${}^{14}\text{N}_2$

Recent analyses of synchrotron-based photoabsorption spectra for the $o\ {}^1\Pi_u-X\ {}^1\Sigma_g^+(2,0)$ band of ${}^{14}\text{N}_2$ have revealed that the $o(v=2)$ level exhibits predissociation linewidths that are indicative of perturbation by a triplet state.⁴⁷ The corresponding reduced term values and linewidths, averaged over the e - and f -parity levels, are shown in Figs. 9(a) and 9(b), respectively (circles). Taken together, the data are consistent with perturbation by a short-lived case-(b) ${}^3\Pi_u$ state, exhibiting three local perturbations which affect both the energies and widths of the $J=14, 16$, and 18 levels of $o(v=2)$, the central $J=16$ level being the least affected. The situation is

very similar to the perturbation of $o(v=0)$ in ${}^{15}\text{N}_2$ by $C(v=13)$ (see Sec. III A 3 and Fig. 4). Here, it is $C(v=18)$ of ${}^{14}\text{N}_2$ that is responsible for the perturbation.²⁴

Spectroscopic parameters for $C(v=18)$ of ${}^{14}\text{N}_2$, deduced by the same procedure as in Sec. III A 3, are summarized in the third column of Table I. The corresponding simultaneously fitted reduced terms and predissociation linewidths, shown as full lines in Figs. 9(a) and 9(b), are in good agreement with the experimental values.

B. The $G\ {}^3\Pi_u$ state

1. $G\ {}^3\Pi_u(v=0)$ in ${}^{14}\text{N}_2$ and ${}^{15}\text{N}_2$

In Fig. 10, the LN_2 -temperature photoabsorption spectrum for ${}^{14}\text{N}_2$, recorded photographically in the region of the $b\ {}^1\Pi_u-X\ {}^1\Sigma_g^+(4,0)$ band, is shown, revealing a region of enhanced absorption containing a dense rotational structure,

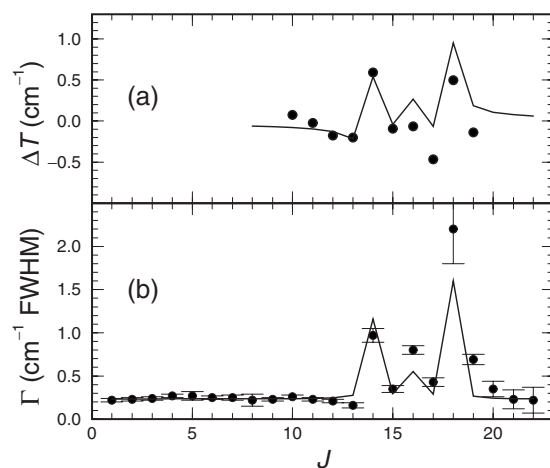


FIG. 9. The local perturbation of $o\ {}^1\Pi_u(v=2)$ of ${}^{14}\text{N}_2$ in the $J=14-18$ region by the higher-lying, shorter-lived $C\ {}^3\Pi_u(v=18)$. Predissociation linewidths and reduced term values from synchrotron-based spectra (Ref. 47), averaged over the e - and f -parity levels (circles), are compared with calculations from a ${}^1\Pi_u \sim {}^3\Pi_u$ interaction model (lines; see text).

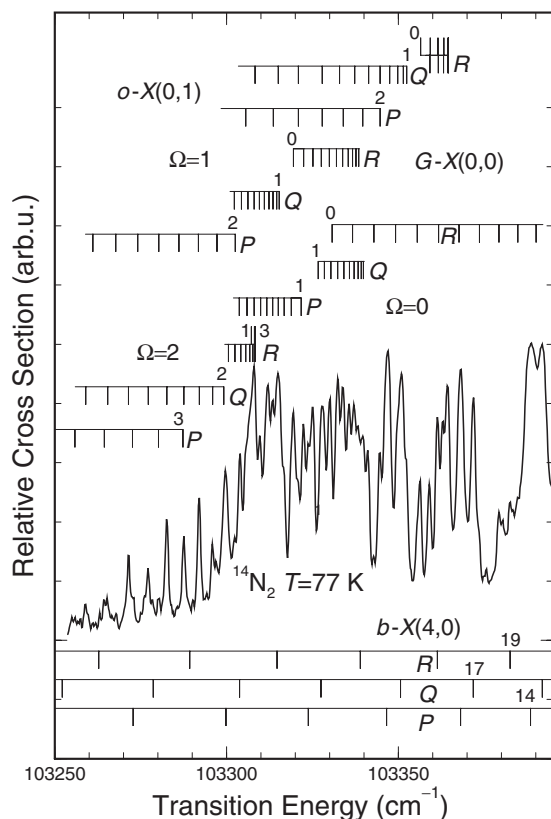


FIG. 10. LN₂-temperature photoabsorption spectrum in the region of the $b\ ^1\Pi_u-X\ ^1\Sigma_g^+(4,0)$ transition of $^{14}\text{N}_2$, obtained from a spectrographic plate, revealing rotational structure due to the $G\ ^3\Pi_{u\Omega}-X\ ^1\Sigma_g^+(0,0)$ transitions. The spectrum is overlapped by additional structure from the $o\ ^1\Pi_u-X\ ^1\Sigma_g^+(0,1)$ transition (Ref. 36).

which represents the first optical observation of the Rydberg $G\ ^3\Pi_{u\Omega}-X\ ^1\Sigma_g^+(0,0)$ EUV transition of N_2 . This observation follows the recent detailed characterization of the $G(v=0)$ state by Hashimoto and Kanamori,²² who performed a near-infrared diode-laser kinetic-spectroscopic study of the $G\ ^3\Pi_{u\Omega}-E\ ^3\Sigma_g^+(0,0)$ transition. Transition energies for $J'' \leq 10$, from the line assignments indicated in Fig. 10, are shown in Table VII, together with the corresponding rotational term values.

Sprengers *et al.*²⁶ reported unattributed local perturbations in both the e - and f -parity levels of $b(v=4)$, near $J = 18$ for $^{14}\text{N}_2$ and $J = 15$ for $^{15}\text{N}_2$. The strongest of these perturbations were also reported by Stark *et al.*,⁴⁸ who observed extra lines associated with the $R(17)$ and $P(19)$ transitions in $^{14}\text{N}_2$. Based mainly on energetic considerations, it is likely that the perturber is the upper ($\Omega=0$) component of the inverted $G\ ^3\Pi_{u\Omega}(v=0)$ state.²² In order to further characterize these perturbations, we have measured additional PDL- and PDA-based ionization spectra. In Figs. 11(a) and 11(b), PDL-based spectra are shown for the $b-X(4,0)$ bands of $^{14}\text{N}_2$ and $^{15}\text{N}_2$, respectively, highlighting the assignments of the narrower extra lines associated with transitions into the $G\ ^3\Pi_{u\Omega}(v=0)$ perturbing state. Corresponding transition energies and rotational terms are also included in Table VII.

Using a four-level least-squares fitting procedure similar to that described in Sec. III A 3, with the inclusion of an effective spin-orbit interaction $H_{G(0)b(4)}$ between the

$b\ ^1\Pi_{u1}(v=4)$ and $G\ ^3\Pi_{u1}(v=0)$ states, the $^{14}\text{N}_2$ terms in Table VII have been deperturbed, yielding the $G(v=0)$ spectroscopic parameters listed in Table VIII. Unfortunately, these parameters cannot be compared easily with the more precise values of Hashimoto and Kanamori,²² who employed a different $^3\Pi$ Hamiltonian and fitted a greater range of rotational levels. However, the present direct determination of the $G-X$ transition energy is consistent with the sum of the $G-E$ energy of Hashimoto and Kanamori²² and the $E-X$ energy given by Carroll and Doheny.⁴⁹ While the corresponding T_0 values given in Table VIII differ by approximately the combined uncertainties, even this small discrepancy disappears completely if individual low- J energy levels are compared directly, indicating consistency between the energy calibrations of the three relevant works. As noted by Hashimoto and Kanamori,²² the high B value for $G(v=0)$ is broadly consistent with expectation for a Rydberg state built on the $X\ ^2\Sigma_g^+$ ionic core ($B_0 = 1.922\ \text{cm}^{-1}$),⁵⁰ and the significant Λ doubling indicated by the large negative value of q can be explained qualitatively by an L -uncoupling interaction with the $D\ ^3\Sigma_u^+(v=0)$ state, which lies just above $G(v=0)$ and is a member of the same $3p$ -Rydberg complex.⁵¹ However, the fact that the B value for $G(v=0)$ is somewhat lower than that of the ionic state on which it is built and the significant negative value of A , which would have been expected to be very small and positive for a pure Rydberg G state,²⁴ suggest a significant degree of mixing with the $F\ ^3\Pi_{u1}(v=0)$ Rydberg state, which is built on the $A\ ^2\Pi_u$ ionic core ($B_0 = 1.735\ \text{cm}^{-1}$).⁵⁰ These aspects have been discussed in detail by Sprengers *et al.*,²³ and the underlying interactions will be addressed further in the companion theoretical study.²⁴

In the current spectra, it has not been possible to detect the local perturbations in $b(v=4)$ caused by the expected crossings at higher J by the $\Omega=1$ and $\Omega=2$ components of the triplet $G(v=0)$ state, due to the apparent weakness of the perturbation and the limited wavelength range scanned, respectively. However, analysis of the $b(v=4)$ terms of Yoshino⁵² for $^{14}\text{N}_2$ indicates clear local perturbations due to the $\Omega=2$ crossing at $J=25e-26e$ and $J=26f-27f$. It should be noted here that using the $G(v=0)$ spectroscopic parameters of Table VIII with the $^3\Pi$ Hamiltonian of Brown and Merer³⁴ fails to reproduce the observed positions of these upper crossings due to a very strong parameter dependence on the range of J levels fitted. This implies that the $G(v=0)$ level is affected by an additional perturbation, possibly due to an electrostatic interaction with the $C(v=12)$ valence level which is expected to lie not too far above. If the $\Omega=0$ and $\Omega=2$ crossings for $^{14}\text{N}_2$ are deperturbed independently using a simple two-level model, the following effective interaction matrix elements are found: $H_{12} = 1.71(9)\ \text{cm}^{-1}$ for $\Omega=0f$, $H_{12} = 1.57(3)\ \text{cm}^{-1}$ for $\Omega=0e$, and $H_{12} = 1.55(15)\ \text{cm}^{-1}$ for $\Omega=2e$, with no determination possible for $\Omega=2f$ due to noisy data. These results are quite consistent with the fitted value of $H_{G(0)b(4)} = 2.17(10)\ \text{cm}^{-1}$ in Table VIII, together with the picture of a $^1\Pi \sim ^3\Pi$ interaction where the $^3\Pi$ state has Hund's case (b) angular-momentum coupling, as detailed, e.g., by Kovacs,³⁹ which

TABLE VII. Observed transition energies and upper-state term values for the $G\ {}^3\Pi_u-X\ {}^1\Sigma_g^+(0,0)$ bands of ${}^{14}N_2$ and ${}^{15}N_2$ from photographic ($J'' \leq 10$) and PDL- and PDA-based spectra. Note that $103\,000\text{ cm}^{-1}$ must be added to the tabulated values.

Isotopomer	Ω'	J''	$R(J'')$	$Q(J'')$	$P(J'')$	J'	$T_e(J')$	$T_f(J')$			
${}^{14}N_2$	0	1				1	330.71 ^a				
		2	342.80 ^b	328.40 ^c	318.77 ^c	2	340.68 ^a	340.34 ^c			
		3			316.80 ^a	3	354.74 ^b				
		4	355.47 ^a	332.40 ^c		4	373.08 ^c	372.19 ^c			
		5		334.18 ^{a,c}	313.41 ^c	5	395.26 ^a	393.85 ^{a,c}			
		6		335.66	311.73 ^c	6	421.18 ^c	419.22			
		7	373.52 ^a	337.08 ^c	309.77 ^c	7		448.49 ^c			
		8	379.27	338.25 ^c		8	484.93 ^a	481.48			
		9	384.68 ^a	339.26 ^c		9	522.50	518.29 ^c			
		10		339.86 ^c		10	563.71 ^a	558.66 ^c			
		15	413.61 ^b								
		16	417.46				16	890.80 ^b			
		17	423.03				17	958.22			
		18			335.43		18	1031.33	1015.22		
		19			334.43	276.10	19		1089.66		
		1	1	0	319.48						
				1	322.40	315.35 ^c		1	319.48	319.33 ^c	
				2	325.08			2	326.38		
				3		313.41 ^c		3	336.90	337.29 ^c	
	4			330.07 ^c	312.06 ^c	296.99	4		351.85 ^c		
	5			332.33 ^c			5	369.86 ^c			
	6			333.86 ^c	309.77 ^c		6	391.84 ^c	393.33 ^c		
	7					280.26 ^c	7	417.42 ^c			
	10				302.25 ^c		10		521.05 ^c		
	2			2	2	308.02 ^c					
					3	308.48 ^c	295.89		3	320.01 ^c	319.77
					4	308.02 ^c	292.04	280.26 ^c	4	332.33 ^c	331.83
					5	306.68 ^c	287.59	272.62 ^c	5	347.94 ^c	347.26
					6	306.59 ^{a,c}	282.65	264.38 ^c	6	367.35 ^c	366.21
		7	305.50 ^{a,c}		277.22		7	390.15 ^{a,c}	388.63		
		8			271.53		8	416.91 ^{a,c}	414.76		
	9	302.25 ^c	265.34 ^c		9		444.37 ^c				
	10		259.02 ^b		10	481.28 ^c	477.82 ^b				
${}^{15}N_2$	0	11	396.26 ^c								
		12	400.89 ^c			12	641.39				
		13	405.25	345.48	303.47	13	690.48	683.40			
		14	408.30	345.13	300.60	14	743.17	735.01			
		15		344.45	297.62	15	798.17	789.99			
		16		344.08 ^b	293.25	16		848.99			

^aFrom a shoulder in the spectrum.

^bFrom a weak line in the spectrum.

^cFrom a blend in the spectrum.

predicts $H_{12}=1.51\text{ cm}^{-1}$ for $\Omega=0$, $H_{12}=0.1\text{ cm}^{-1}$ for $\Omega=1$, and $H_{12}=1.55\text{ cm}^{-1}$ for $\Omega=2$, thus explaining the absence of a measurable $\Omega=1$ perturbation.⁵³

In the case of ${}^{15}N_2$, the limited number of $G(v=0)$ levels discovered here does not justify the fitting of a full ${}^3\Pi$ Hamiltonian. However, separate local deperturbations of the $\Omega=0$ crossings yield the following interaction matrix elements: $H_{12}=1.5(1)\text{ cm}^{-1}$ for $\Omega=0f$ and $H_{12}=1.63(5)\text{ cm}^{-1}$ for $\Omega=0e$, very similar to those found for ${}^{14}N_2$.

Particularly noticeable in Fig. 11(b) is the remarkable strength of the extra lines in ${}^{15}N_2$ when compared with the main lines. For example, in the case of the $Q(15)$ transition, the extra line is nearly four times stronger than the main line, from which it borrows its absorption strength through spin-

orbit coupling. The explanation for this interesting phenomenon lies in the competition between ionization and predissociation in these laser-based spectra, with the $G(v=0)$ predissociation linewidths in ${}^{15}N_2$ in the region of the perturbation clearly much narrower than those for $b(v=4)$, implying a substantially longer decay lifetime and corresponding increase in the ionization signal for the $G(v=0)$ levels. In the case of ${}^{14}N_2$, the same phenomenon occurs, but to a much smaller extent. Direct lineshape fitting to the $R(13)$, $P(15)$, and $Q(15)$ lines from the PDA-based ${}^{15}N_2$ spectra of this work yields conservative upper limits to the level widths of 0.005 cm^{-1} FWHM and 0.01 cm^{-1} FWHM, respectively, for $J=14e$ and $J=15f$. On the other hand, refitting the $R(17)$ extra line in the ${}^{14}N_2$ photoabsorption spectra of Stark

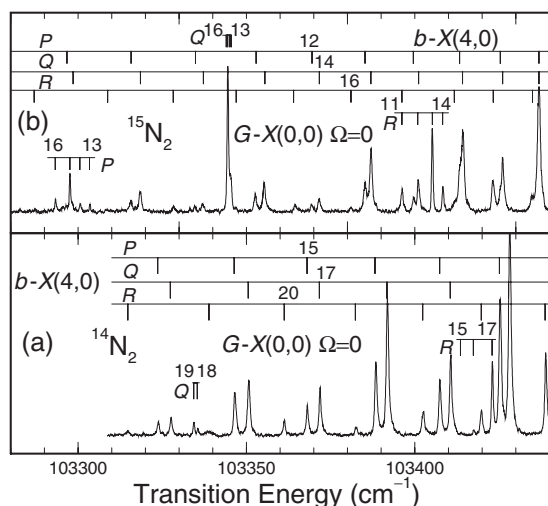


FIG. 11. One EUV+one UV ionization spectra of the $b^1\Pi_u-X^1\Sigma_g^+(4,0)$ bands in (a) $^{14}\text{N}_2$ and (b) $^{15}\text{N}_2$, recorded with the PDL-based EUV source. Extra lines associated with the $G^3\Pi_u-X^1\Sigma_g^+(0,0)$ transition are indicated.

et al.,⁴⁸ corresponding to the region of maximum perturbation, yields a much larger width of $0.082(16) \text{ cm}^{-1}$ FWHM for $J=18e$.

2. $G^3\Pi_u(v=1)$ in $^{14}\text{N}_2$

In Fig. 12, the LN₂-temperature spectrum for $^{14}\text{N}_2$, recorded photographically in the region just above the *R* head of the $b-X(7,0)$ band, is shown, revealing a very weak, diffuse absorption feature near $106\,160 \text{ cm}^{-1}$. The KER spectra of van der Kamp *et al.*,²¹ resulting from N_2^+ dissociative charge transfer in Cs vapor, display an unassigned peak $484(60) \text{ cm}^{-1}$ above the peak associated with $o^1\Pi_u(v=0)$ of $^{14}\text{N}_2$. The energy of the latter has long been established at $105\,683 \text{ cm}^{-1}$,⁵⁴ thus placing the unassigned peak at $106\,167 \text{ cm}^{-1}$, i.e., at 195 cm^{-1} above the energy originally

TABLE VIII. Spectroscopic parameters, in cm^{-1} , for the deperturbed $G^3\Pi_u(v=0)$ level of $^{14}\text{N}_2$. 1σ statistical uncertainties resulting from the fitting procedure are given in parentheses, in units of the last significant figure.

Parameter	This work	Ref. 22
ν_0 ^a	103 313.7(2)	
T_0 ^b	103 317.1(3)	103 317.39(5) ^c
B	1.867(1)	
D	$1.6(5) \times 10^{-5}$	
A	-8.35(8)	
A_D	-0.042(7)	
λ	0.0 ^d	
λ_D	0.007 6(18)	
γ	0.15(4)	
o	0.05(6)	
p	0.009(7)	
q	-0.043(2)	
$H_{G(0)b(4)}$	2.17(10)	
σ_{fit}	0.086	

^aTabulated uncertainties include the calibration uncertainty.

^bRotationless F_2 energy = $\nu_0 - 4\lambda/3 + 2(B - 4\lambda_D/3) - 2\gamma$.

^c $[G-E(0,0)] + [E-X(0,0)]$; see Refs. 22 and 49.

^dParameter fixed during fitting procedure.

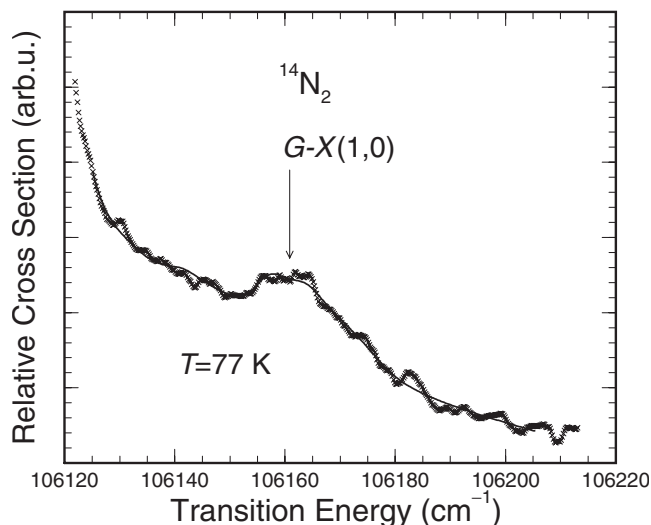


FIG. 12. LN₂-temperature photoabsorption spectrum (crosses) for the diffuse $G^3\Pi_u-X^1\Sigma_g^+(1,0)$ band of $^{14}\text{N}_2$, which appears as a shoulder on the $b^1\Pi_u-X^1\Sigma_g^+(7,0)$ band head, obtained from a spectrographic plate. Some sharp discrete features have been removed from the spectrum for clarity. Also shown is the result of a band-model fit (solid curve; see text).

determined by van der Kamp *et al.*²¹ The difference results from our recalibration of the KER spectrum on the basis of a progression of $o^1\Pi_u$ levels and the newly established energies for $G^3\Pi_u(v=0)$ and $F^3\Pi_u(v=0)$.²³ Their peak at $106\,167 \text{ cm}^{-1}$ coincides nearly perfectly with the diffuse peak in Fig. 12, and the CSE-model calculations in the following paper by Lewis *et al.*²⁴ leave no doubt that it is associated with the $G^3\Pi_u(v=1)$ Rydberg state. On intensity grounds, a $G(v=1)$ peak is certainly expected to have been observable in the KER spectra of Ref. 21.

It follows that the diffuse feature in Fig. 12 represents the first optical observation of the Rydberg $G^3\Pi_u-X^1\Sigma_g^+(1,0)$ dipole-forbidden transition. Because of the weakness and diffuseness of this band, normal spectroscopic analysis is impossible. However, if it is assumed that the B and A values for $G(v=1)$ are similar to those for $G(v=0)$, discussed in Sec. III B 1, and that the branch intensity structure is driven principally by intensity borrowing from the nearby $b-X(7,0)$ dipole-allowed transition, mediated by the $b^1\Pi_{u1}(v=7) \sim G^3\Pi_{u1}(v=1)$ spin-orbit coupling, then it is feasible to perform a limited Lorentzian-profile-based band-model fit to the observed spectrum. The results of such a fit, in which only the origin, overall intensity, (J -independent) linewidth, and background polynomial terms were permitted to vary, are shown as the solid line in Fig. 12, seen to be in good agreement with the measurements (crosses). The important fitted results for $G(v=1)$ of $^{14}\text{N}_2$ are $\nu_0 = 106\,163(1) \text{ cm}^{-1}$ and $\Gamma = 9.6(12) \text{ cm}^{-1}$ FWHM.

C. The $F^3\Pi_u$ state

1. $F^3\Pi_u(v=0)$ in $^{14}\text{N}_2$

The Rydberg $F(v=0)$ state was first assigned correctly in the low-resolution translational-spectroscopic study of Ref. 21. Here, we have observed the $F-X(0,0)$ band of $^{14}\text{N}_2$ photographically and also in a higher-resolution PDA-based laser-spectroscopic study, the results of which have been re-

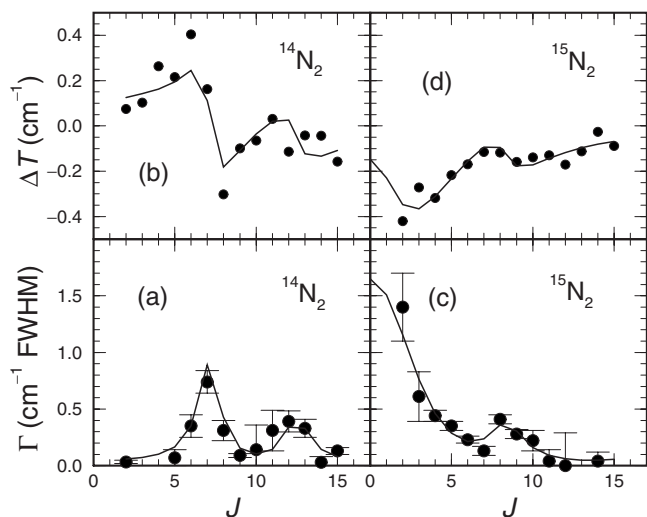


FIG. 13. The perturbation of $b' {}^1\Sigma_g^+(v=4)$ by the lower-lying, shorter-lived $F {}^3\Pi_u(v=1)$ state. Observed predissociation linewidths and reduced term values (circles) are compared with the results of a four-level deperturbation (lines; see text).

ported elsewhere.²³ The reader is referred to Ref. 23 for a discussion of the $F(v=0)$ spectroscopic parameters and predissociation linewidths.

2. $F {}^3\Pi_u(v=1)$ in ${}^{14}N_2$ and ${}^{15}N_2$

In a synchrotron-based EUV photoabsorption study of ${}^{14}N_2$, performed using the 6.65 m spectrometer at the Photon Factory (Tsukuba, Japan), Stark *et al.*⁴⁸ reported noticeable predissociation broadening of the $b' {}^1\Sigma_u^+(v=4)$ levels near $J=7$. In the light of this observation, we have reanalyzed the $b'-X(4,0)$ spectra of Ref. 48, extending the profile-fitting analyses to $J=15$. The resultant predissociation linewidths, shown in Fig. 13(a) (circles), including an additional point at $J=2$ from the much higher-resolution study of Ref. 29, display a double-peaked structure with maxima at $J=7$ and $J=12-13$. The corresponding $b'(v=4)$ reduced term values, shown in Fig. 13(b) (circles), indicate that the $J=7$ peak in Fig. 13(a) is associated with a local perturbation by a state having a higher rotational constant, but the scatter in the data does not allow the observation of any energy perturbation associated with the second width peak in Fig. 13(a). Sprengers *et al.*²⁶ previously reported PDL-based $b'-X(4,0)$ ionization spectra for ${}^{15}N_2$, concentrating on the determination of term values. Here, we have extended their analyses to include line-profile fitting, obtaining the corresponding predissociation linewidths and reduced term values shown in Figs. 13(c) and 13(d), respectively (circles). The heavier isotopomer displays behavior similar to that observed for ${}^{14}N_2$, with a strong width peak, albeit not well defined, near $J \leq 2$ and a secondary peak at $J=8-9$. In this case, however, while the stronger, low- J local energy perturbation is not defined completely, the second, weaker perturbation from below at $J=8-9$ is evident due to reduced scatter in the experimental terms.

Taken together, the results of Fig. 13 suggest that $b'(v=4)$ is perturbed by a short-lived, lower-lying *ungerade* multiplet state, probably of Rydberg type, with an $\Omega=0$ upper

TABLE IX. Spectroscopic parameters, in cm^{-1} , for the deperturbed $F {}^3\Pi_u(v=1)$ levels of ${}^{14}N_2$ and ${}^{15}N_2$, assuming no Λ doubling. 1σ statistical uncertainties resulting from the fitting procedure are given in parentheses, in units of the last significant figure.

Parameter	$F(v=1), {}^{14}N_2$	$F(v=1), {}^{15}N_2$
ν_0	106 577(2)	106 534(3)
T_0^a	106 579(2)	106 537(3)
B	1.75(3)	1.61(4)
D	$3 \times 10^{-5}{}^b$	$3 \times 10^{-5}{}^b$
A	-28(3)	-32(2)
λ	0.5 ^b	0.5 ^b
$H_{F(1)b'(4)}$	2.1(2)	2.7(1)
Γ^c	16(3)	18(2)
σ_{fit}	0.091	0.074

^aRotationless F_2 energy = $\nu_0 - 4\lambda/3 + 2B$.

^bParameter fixed during fitting procedure.

^cFWHM predissociation linewidth.

component. The KER spectra of van der Kamp *et al.*²¹ position the $F {}^3\Pi_u(v=1)$ level of ${}^{14}N_2$ at 106 384 cm^{-1} . Our recalibration of their KER spectrum (see Sec. III C of the following paper) increases this energy to 106 578(60) cm^{-1} , just below the $b'(v=4)$ level at 106 647 cm^{-1} . Therefore, we have simultaneously deperturbed the $b'(v=4)$ terms and widths using a four-level model including the $F {}^3\Pi_u(v=1)$ Rydberg and $b' {}^1\Sigma_u^+(v=4)$ valence states, together with an effective spin-orbit interaction matrix element $H_{F(1)b'(4)}$ between the $\Omega=0$ components.

The unperturbed $b'(v=4)$ levels were taken to be unperturbed, with terms described by a cubic polynomial in $J(J+1)$, while the unperturbed predissociation width for the $F {}^3\Pi_u(v=1)$ state, assumed to have no Ω or J dependence, was included as a complex term in the diagonal energy matrix. In this approximation, the resultant predissociation width for the $b'(v=4)$ level arises only through borrowing from the $F {}^3\Pi_u(v=1)$ state.

The fitted deperturbed $F {}^3\Pi_u(v=1)$ spectroscopic parameters for ${}^{14}N_2$ and ${}^{15}N_2$ are listed in Table IX, with the corresponding fitted widths and reduced terms, shown in Fig. 13 (curves), in excellent agreement with the experimental values (circles). Despite the lack of direct observations, it is still possible to glean spectroscopic information on the F state, albeit with a significantly increased level of uncertainty. The fitted band-origin isotopic shift, 43(4) cm^{-1} , is consistent with expectation for the $v=1$ level of a Rydberg state built on the $A {}^2\Pi_u$ state of N_2^+ ,⁵⁵ confirming the vibrational assignments of Ref. 21, while the ratio of the rotational constants $B_{15}/B_{14}=0.92(5)$, in agreement with the ratio of 0.93 expected from normal reduced-mass considerations.⁵⁶ The fitted A values for each isotopomer are in agreement within the combined uncertainties. It is of interest that the mean value of $|A| \approx 30$ cm^{-1} is significantly greater in magnitude than the value of 21.82(1) cm^{-1} reported for the $F(v=0)$ level by Sprengers *et al.*²³ and closer to the value of ~ 37 cm^{-1} that would be expected for an unperturbed Rydberg state converging on the $A {}^2\Pi_u$ state of N_2^+ .²³ This suggests a significantly smaller G -state admixture in $F(v=1)$ than that found previously for $F(v=0)$.²³ Finally, the fitted predissociation widths for each isotopomer are in agreement within the com-

bined uncertainties. The mean value, $\Gamma(F) \approx 17 \text{ cm}^{-1}$ FWHM, indicates very strong predissociation, supporting the important role of the ${}^3\Pi_u$ states in controlling the predissociation routes for the singlet states of N_2 .

IV. SUMMARY AND CONCLUSIONS

High-resolution laser-based one EUV+one UV two-photon ionization spectroscopy and EUV photoabsorption spectroscopy have been employed to study spin-forbidden ${}^3\Pi_u$ - $X^1\Sigma_g^+$ transitions in ${}^{14}\text{N}_2$ and ${}^{15}\text{N}_2$. Levels of the $C^3\Pi_u$ valence and F and $G^3\Pi_u$ Rydberg states have been characterized, either through their direct optical observation, or, indirectly, through their perturbative effects on the ${}^1\Pi_u$ and ${}^1\Sigma_u^+$ states, which are accessible in dipole-allowed transitions. Optical observation of the G - $X(0,0)$ and $(1,0)$ transitions is reported for the first time, together with evidence for six new vibrational levels of the C state. Despite their somewhat fragmentary nature, these new observations provide a valuable database on the ${}^3\Pi_u$ states of N_2 and their interactions, which is employed in the following companion paper in this issue²⁴ to inform the development of a CSE model of the interacting ${}^3\Pi_u$ states of N_2 , and which will help elucidate the predissociation mechanisms for the nitrogen molecule.

ACKNOWLEDGMENTS

This work was partially supported by Australian Research Council Discovery Program Grant Nos. DP0558962 and DP0773050, NASA Grant No. NNG05GA03G, and the Molecular Atmospheric Physics program of the Netherlands Foundation for Fundamental Research on Matter. K.G.H.B. was supported by the Scientific Visits to Europe Program of the Australian Academy of Science. J.P.S. thanks the ANU for the hospitality enjoyed during visits to Canberra. We also thank Professor H el ene Lefebvre-Brion and Professor Roland Lefebvre for the provision of a program for the diagonalization of complex matrices.

¹H. Lefebvre-Brion, *Can. J. Phys.* **47**, 541 (1969).

²K. Dressler, *Can. J. Phys.* **47**, 547 (1969).

³P. K. Carroll and C. P. Collins, *Can. J. Phys.* **47**, 563 (1969).

⁴D. Stahel, M. Leoni, and K. Dressler, *J. Chem. Phys.* **79**, 2541 (1983).

⁵J. M. Robbe, Ph.D. thesis, University of Lille, 1978.

⁶B. R. Lewis, S. T. Gibson, W. Zhang, H. Lefebvre-Brion, and J.-M. Robbe, *J. Chem. Phys.* **122**, 144302 (2005).

⁷V. E. Haverd, B. R. Lewis, S. T. Gibson, and G. Stark, *J. Chem. Phys.* **123**, 214304 (2005).

⁸S. G. Tilford, J. T. Vanderslice, and P. G. Wilkinson, *Astrophys. J.* **142**, 1203 (1965).

⁹J. W. Ledbetter, Jr., *J. Chem. Phys.* **67**, 3400 (1977).

¹⁰P. K. Carroll, *Proc. R. Soc. London, Ser. A* **272**, 270 (1962).

¹¹J. W. Ledbetter, Jr. and K. Dressler, *J. Mol. Spectrosc.* **63**, 370 (1976).

¹²Y. Tanaka and A. S. Jursa, *J. Opt. Soc. Am.* **51**, 1239 (1961).

¹³P. K. Carroll and R. S. Mulliken, *J. Chem. Phys.* **43**, 2170 (1965).

¹⁴T. Hori and T. Endo, *Proc. Phys. Math. Soc. Jpn.* **23**, 834 (1941).

¹⁵A. Lofthus and P. H. Krupenie, *J. Phys. Chem. Ref. Data* **6**, 113 (1977).

¹⁶M. Leoni and K. Dressler, *Z. Angew. Math. Phys.* **22**, 794 (1971).

¹⁷P. K. Carroll, C. C. Collins, and J. T. Murnaghan, *J. Phys. B* **5**, 1634 (1972).

¹⁸J. Mazeau, R. I. Hall, G. Joyez, M. Landau, and J. Reinhardt, *J. Phys. B* **6**, 873 (1973).

¹⁹G. Joyez, R. I. Hall, J. Reinhardt, and J. Mazeau, *J. Electron Spectrosc. Relat. Phenom.* **2**, 183 (1973).

²⁰P. Hammond, G. C. King, J. Jureta, and F. H. Read, *J. Phys. B* **20**, 4255 (1987).

²¹A. B. van der Kamp, P. C. Cosby, and W. J. van der Zande, *Chem. Phys.* **184**, 319 (1994).

²²T. Hashimoto and H. Kanamori, *J. Mol. Spectrosc.* **235**, 104 (2006).

²³J. P. Sprengers, E. Reinhold, W. Ubachs, K. G. H. Baldwin, and B. R. Lewis, *J. Chem. Phys.* **123**, 144315 (2005).

²⁴B. R. Lewis, A. N. Heays, S. T. Gibson, H. Lefebvre-Brion, and R. Lefebvre, *J. Chem. Phys.* **129**, 164306 (2008).

²⁵Preliminary results from the C - $X(7,0)$ and $(8,0)$ spectra presented here have already been used in the development of the CSE model of Ref. 6.

²⁶J. P. Sprengers, W. Ubachs, K. G. H. Baldwin, B. R. Lewis, and W.- . L. Tchang-Brillet, *J. Chem. Phys.* **119**, 3160 (2003).

²⁷J. P. Sprengers, W. Ubachs, and K. G. H. Baldwin, *J. Chem. Phys.* **122**, 144301 (2005).

²⁸J. Philip, J. P. Sprengers, P. Cacciani, C. A. de Lange, and W. Ubachs, *Appl. Phys. B: Lasers Opt.* **78**, 737 (2004).

²⁹J. P. Sprengers and W. Ubachs, *J. Mol. Spectrosc.* **235**, 176 (2006).

³⁰M. L. Ginter, D. L. Ginter, and C. M. Brown, *Appl. Opt.* **27**, 4712 (1988).

³¹H. D. Morgan, J. D. E. Fortna, H. M. Seyoum, M. L. Furst, L. R. Hughey, D. C. Humm, and A. Asfaw, *Nucl. Instrum. Methods Phys. Res. A* **347**, 287 (1994).

³²H. Partridge, personal communication (March, 1998).

³³H. H. Michels, *Adv. Chem. Phys.* **45**, 225 (1981).

³⁴J. M. Brown and A. J. Merer, *J. Mol. Spectrosc.* **74**, 488 (1979).

³⁵It was assumed that $A > 0$ for this relatively low level of the C state, i.e., of the same sign as the values determined for all known lower- v levels (Ref. 8).

³⁶Despite the low temperature of the absorbing N_2 , hot bands also appear in the recorded spectra. This occurs because of the placement of the windowless absorption cell between the discharge source and the spectrograph, which results in some vibrationally excited N_2 in the absorption path.

³⁷The $R(2)$ and $R(3)$ lines of the o - $X(0,0)$ band coincide due to an additional perturbation by the $D(v=1)$ state.

³⁸The ${}^{15}\text{N}_2$ $o(v=0)$ terms of Ref. 26 were supplemented by a $T_e(15)$ value of $106\,019.555 \text{ cm}^{-1}$, from a new assignment of a shoulder in the spectrum to $R(14)$.

³⁹I. Kovacs, *Rotational Structure in the Spectra of Diatomic Molecules* (Hilger, London, 1969), pp. 272–274.

⁴⁰A few preliminary results from the PDA-based study have been presented in Ref. 29.

⁴¹J. Bendtsen, *J. Raman Spectrosc.* **32**, 989 (2001).

⁴²Term-value fits for A chosen to be positive or negative both imply that A_D/A is negative. The inverted $F^3\Pi_u(v=1)$ level, which lies $\sim 60 \text{ cm}^{-1}$ above $C^3\Pi_u(v=14)$ (see Sec. III C 2), perturbs its spectroscopic constants electrostatically. Since the Rydberg $F(v=1)$ state has larger values of $|A|$ and B than those of the valence $C(v=14)$ state, the observed $A_D/A < 0$ implies that $A < 0$ for the latter state. If A were positive, then this perturbation would result in A_D/A having quite a large positive value and λ probably being of opposite sign to that observed.

⁴³H. Ndome, M. Hochlaf, B. R. Lewis, A. N. Heays, S. T. Gibson, and H. Lefebvre-Brion, *J. Chem. Phys.* **129**, 164307 (2008).

⁴⁴For this conclusion, it is assumed that predissociation is the dominant decay process.

⁴⁵J. P. Sprengers, A. Johansson, A. L'Huillier, C.-G. Wahlstr om, B. R. Lewis, and W. Ubachs, *Chem. Phys. Lett.* **389**, 348 (2004).

⁴⁶At LN_2 temperature, the $Q(2)$ line from a ${}^1\Pi_u$ - $X^1\Sigma_g^+$ transition, or a central subband ${}^3\Pi_{u1}$ - $X^1\Sigma_g^+$ transition which borrows strength from this allowed transition, is significantly stronger than the $R(4)$ line. However, the ${}^3\Pi_{u0} \sim {}^3\Pi_{u1}$ rotational mixing is strongly J dependent, resulting in the $R(4)$ line becoming significantly stronger than the $Q(2)$ line in the ${}^3\Pi_{u0}$ - $X^1\Sigma_g^+$ subband.

⁴⁷G. Stark, B. R. Lewis, A. N. Heays, K. Yoshino, P. L. Smith, and K. Ito, *J. Chem. Phys.* **128**, 114302 (2008).

⁴⁸G. Stark, K. P. Huber, K. Yoshino, P. L. Smith, and K. Ito, *J. Chem. Phys.* **123**, 214303 (2005).

⁴⁹P. K. Carroll and A. P. Doheny, *J. Mol. Spectrosc.* **50**, 257 (1974).

⁵⁰K. P. Huber and G. Herzberg, *Molecular Spectra and Molecular Structure IV. Constants of Diatomic Molecules* (Van Nostrand, New York, 1979), p. 426.

⁵¹H. Lefebvre-Brion and R. W. Field, *The Spectra and Dynamics of Diatomic Molecules* (Elsevier, Amsterdam, 2004), pp. 399–400.

⁵²K. Yoshino (<http://cfa-www.harvard.edu/amp/ampdata/cfamols.html>).

⁵³While no local perturbation was observed corresponding to the expected $b\ {}^1\Pi_u(v=4) \sim G\ {}^3\Pi_u(v=0)$ crossing, a single perturbation at $J=22e$, with $H_{12}=0.40(2)\text{ cm}^{-1}$, was found, which we believe to be caused by an additional crossing by the $b'\ {}^1\Sigma_u^+(v=0)$ state.

⁵⁴K. Yoshino, Y. Tanaka, P. K. Carroll, and P. Mitchell, *J. Mol. Spectrosc.* **54**, 87 (1975).

⁵⁵Using the ω_e and $\omega_e x_e$ values for the $A\ {}^2\Pi_u$ state of N_2^+ and the $X\ {}^1\Sigma_g^+$ state of N_2 given in Ref. 15, together with the usual isotopic relation (Ref. 56), one finds an $A-X(1,0)$ isotopic shift of $\sim 55\text{ cm}^{-1}$. The actual shift for $F-X(1,0)$ differs somewhat because of the strong interactions within the ${}^3\Pi_u$ manifold of N_2 .

⁵⁶G. Herzberg, *Molecular Spectra and Molecular Structure I. Spectra of Diatomic Molecules* (Van Nostrand, Princeton, 1950), pp. 141–145.